Supporting Information

Upcycled Ni-Co-Mn oxide bifunctional electrocatalyst from spent LIBs for electrochemical water splitting

Divyani Gupta[≠,a] Jingxiu Wang[≠,a] Huaxuan Han,[a] Yan Wang,[a] Anoja Kawsihan,[a]Fangli Zhang,[b] Gemeng Liang,[a] Jianfeng Mao,[a] Jinshuo Zou*[,a]

[a] *School of Chemical Engineering, Adelaide University, Adelaide, SA-5005, Australia*

[b] *School of Science, RMIT University, Melbourne, Victoria, Australia.*

* Corresponding author.

≠ These authors contributed equally to this work.

Experimental Section

Materials and chemicals

Materials. The spent black mass was provided by Iondrive Technologies. The optimized leaching conditions were based on our previous work.[1] Both the black mass and the leaching residue were determined after digestion in aqua regia (concentrated HCl: HNO_3 at 3:1 ratio) followed by ICP-MS analysis.

Chemicals. Choline chloride (ChCl, ≥98%), lactic acid (LA, ≥85%), and L-ascorbic acid (Vitamin C, ≥99%) were purchased from Sigma-Aldrich. All chemicals were of analytical grade and used as received without further purification.

The analytical grade chemicals used during electrochemical tests *i.e.* potassium hydroxide (KOH, 88 %) and sodium chloride (NaCl) were purchased from Sigma Aldrich and used as such without further purification. Deionized water was obtained from a Millipore system (>14 MΩ cm^{-1}), Nafion membrane (Nafion®117) was purchased from FuelCellsEtc. and carbon paper substrate was procured from Fuel cell store.

Preparation of deep eutectic solvent

The binary DES was prepared by mixing ChCl and LA at a molar ratio of 1:10 in a sealed glass vial. The mixture was heated at 60 °C under stirring until a clear, homogeneous liquid was formed and subsequently cooled to room temperature. Before use, 1% (w/v) L-ascorbic acid (VC) was added to the mixture and stirred at 60 °C until fully dissolved, yielding the ternary DES (1ChCl–10LA–VC).

Leaching of Black Mass and Synthesis of NiCoMn Catalysts

For leaching, 100 mg of NCM black mass was added to 5 mL of the prepared DES in a glass reactor. The mixture was heated at 60 °C and stirred for 8 h to achieve selective dissolution of Li while retaining transition metals in the solid phase. After leaching, the suspension was filtered to collect the DES leachate and the solid residue.[1]

The residue enriched in Ni, Co, and Mn was washed thoroughly with ethanol to remove residual DES, then dried at 80 °C overnight. The dried residue was calcined in a muffle furnace at 700, 800, or 900 °C to obtain the corresponding NiCoMn oxide catalysts. These catalysts were subsequently subjected to detailed structural and chemical characterization.

Materials characterizations

X-ray diffractometer (XRD). Phase identification of calcined products was performed using a Rigaku MiniFlex 600 diffractometer (Japan) equipped with Cu Kα radiation (λ = 1.54056 Å) in the 2θ range from 5 to 80 degree.

Raman Spectroscopy. Raman spectra were collected using a Horiba LabRAM HR Evolution microscope with a 532 nm excitation laser. A 50× objective was used for focusing and an 1800 gr/mm grating for spectral acquisition over 400–4000 cm^{-1}. To avoid thermal damage, the laser power was set to 100 mW, with an exposure time of 30 s and 5 accumulations for each spectrum.

X-ray photoelectron spectroscopy (XPS). The surface chemical states of Ni, Co, and Mn were analysed using Nexsa surface analysis system (ThermoFisher SCIENTIFIC) with an Al Kα ***excitation*** source (hν = 1486.6 eV) at the vacuum of 1×10^{-8} Pa. The measurements were performed in fixed transmission mode to obtain Co 2p, Ni 2p, Mn 2p and O 1s spectra. Binding energies were calibrated to the C 1s peak at 284.8 eV and deconvolution was performed using CasaXPS Version 2.3.16 software.

Scanning electron microscopy (SEM). The micromorphology of the calcined catalysts was examined using JEOL JSM-7100F (Zeiss SIGMA FESEM, Germany) operated at 18 kV accelerating voltage.

Transmission electron microscopy (TEM). TEM measurements were conducted using the Philips CM200 TEM operating at 200 kV with maximum resolution of 0.2nm and magnification up to 2,000,000x.

Water contact angle measurements. Static water contact angles were measured at room temperature using a Biolin Scientific Theta T200 optical contact angle analyser. The powder samples were pressed into flat circular pellets to obtain a smooth surface. A 3 µL droplet of deionised water was gently placed on the sample surface and images were recorded after the droplet stabilised. Contact angles were determined by fitting the droplet profile using the Young–Laplace equation in the OneAttension software.

In-situ synchrotron FTIR. In-situ synchrotron-FTIR measurements were conducted at the infrared beamline of Australian Synchrotron Centre using a customized home-made electrochemical cell equipped with a ZnSe crystal as the IR transmission window (cut-off energy ~625 cm^{-1}). The data was recorded in a reflectance mode with a vertical incidence of infrared light (opticfibre source) on the working electrode during measurement using a 20x objective within mid-IR spectral region (3950-950 cm^{-1}), 4 cm^{-1} resolution and 512 co-added scans in form of single-point difference spectra. A three-electrode assembly was utilized to conduct the OER and HER experiments (in 1 M KOH), comprising catalyst coated carbon paper as working electrode, Hg/HgO as the reference electrode and a Pt wire as counter electrode, respectively. The electrochemical cell was connected to CHI potentiostat to apply the respective potentials. Background spectra were collected using the same acquisition parameters and cell setup prior to commencing the reaction through applied potentials at open-circuit potentials. It is important to highlight the possible interferences from the water and CO_2 molecules during spectra acquisition can result in reduced transmission of IR light and obscure important spectral details, requiring pre- and post-processing methods.[2, 3] Excessive water absorption was prevented by carefully maintaining the gap between Ge ATR crystal and working electrode on the order of microns and collecting the background FTIR data through the air followed by 10-20 different measurement points across the sample surface. This approach eliminated the need to move the ATR crystal back and forth between background and sample, leading to a faster scan and minimized contamination in background spectrum. Before each measurement, the background spectrum of working electrode was acquired at open-circuit potential, with the cell filled with electrolyte under no applied potential. The data was further analyzed and processed using OPUS and Origin software packages by means of basic spectral manipulation (e.g. baseline correction, atmospheric

correction and normalization) as well as more sophisticated approaches (e.g. spectral deconvolution).

Electrochemical characterizations.

Electrochemical analysis. Electrochemical half-cell tests were performed in a single compartment three-electrode cell setup equipped with a working electrode (WE), Hg/HgO/1 M NaOH as a reference electrode (RE) and Pt wire/graphite rod as a counter electrode (CE). For full-cell water splitting experiments, an H-cell assembly separated by Nafion membrane was utilized. Nafion membrane was cleansed using a three-step procedure involving boiling in deionized water (0.5 h), hydrogen peroxide (H_2O_2 (5%), 0.5 h) and 0.05 M H_2SO_4 (1 h) at 80 °C, respectively, followed by rinsing with fresh deionized water. A catalyst coated carbon paper (0.5 × 0.5 cm^2) was used as a working electrode for electrochemical analyses *viz.* linear sweep voltammetry (LSV), cyclic voltammetry (CV), chronopotentiometry (CP), electrochemical impedance spectroscopy (EIS), *etc.* The catalyst ink was prepared by homogeneously grinding the NCMO-T catalysts (5 mg) using a mortar pestle for 1 hour and later dispersed in isopropyl alcohol (IPA, 80 µL), 5% Nafion solution (20 µL) and deionized water (900 µL, 12 MΩ). The catalyst ink dispersion was then ultrasonicated for 30 min. to obtain a uniform dispersion. 100 µL of the as-prepared catalyst ink was coated over the bare carbon paper substrate via drop-casting method and kept for drying under air overnight. Experiments were performed using a CHI-760E electrochemical workstation and analysed using CHI software. The measurements were performed in 1 M KOH and 1 M KOH + 0.5 M NaCl solutions.

iR-correction procedure. All half-cell electrochemical measurements for the oxygen evolution reaction (OER) and hydrogen evolution reaction (HER) were conducted with 99% iR-compensation applied. The same compensation settings were maintained across all catalysts and electrolytes to ensure consistent comparison. Automatic iR-compensation was performed using a CHI potentiostat. The uncompensated solution resistance (R_u) was determined using the positive-feedback method implemented in the instrument software, where a small potential perturbation (at a non-faradaic potential) with an amplitude of 0.05 V was applied to calculate R_u. Subsequently, 99% of the measured R_u value was compensated during polarization measurements.

Tafel analysis. Tafel slope values were calculated to understand the electrochemical kinetics of catalysts during both HER and OER by plotting Tafel plots between potential (V *vs.* RHE) and log j (current density in mA cm^{-2}), from corresponding LSVs. The slope of linear fit in Tafel plots directly gives the Tafel slope values in mV dec^{-1}.

Electrochemical impedance measurements. The interfacial resistance at electrode-electrolyte interface was measured by performing electrochemical impedance spectroscopy at a fixed OER and HER potentials of 1.56 and -0.2 V *vs.* RHE, respectively, between 10000 Hz and 1 Hz with DC potential over an AC perturbation of 5 mV at a logarithmic frequency step over a single sine wave. Nyquists plots were acquired for all catalytic variants and fitted with

equivalent circuit [R_s + (CPE_1/R_{ct1} + (CPE_2/R_{ct2}))] for OER and [Rs + (CPE‖Rct) + W] for HER, to calculate solution resistance (R_s) and charge transfer resistance (R_{ct}).

Electrochemical surface area (ECSA). The electrochemical surface area was calculated for as-designed catalysts to get insights into the actual exposed and electrochemically active sites during water splitting by determining the double-layer pseudo-capacitance (C_{dl}). Cyclic voltammograms were acquired in the non-faradaic region between 1.03 to 1.23 V *vs.* RHE at various scan rates from 10 to 200 mV s^{-1}. Thereafter, a linear plot between scan rate and averaged out current density at 1.1 V *vs.* RHE (anodic (I_a) and cathodic (I_c) currents, (I_a+I_c)/2) were used to calculate the pseudo-capacitance from its slope. To estimate the ECSA value, the as-obtained C_{dl} was divided by the specific capacitance of the flat surface (20-60 µF cm−2), which in this case is taken as 40 µF cm^{-2}.

Quantification of O_2 and H_2 by Gas chromatography

GC measurements. Gaseous O2 and H2 products formed during OER and HER, respectively, were detected and quantified using a gas chromatograph (Agilent 8890 GC system) with a flame ionization detector (FID) and a thermal conductivity detector (TCD). Chronoamperometry tests were conducted over NCMO-800 catalyst during OER (1.8 V vs. RHE) and HER (-0.5 V vs. RHE), for a fixed duration of 0.5 h by using a half-cell three electrode cell assembly. After 0.5 h, gas sample was collected from headspace of cell and automatically injected into GC column to obtain corresponding chromatogram with % concentration of gaseous products generated using Agilent OpenLab software.

Calculations. The amount of O_2 and H_2 were calculated using below mentioned formulas:

Volume of H_2/O_2 from GC:

To calculate volume of products, following formula is used;

$$V_{product} = V_{loop} \times C_{product} \quad (1)$$

where, $C_{product}$ is the concentration of gaseous product (in %) from GC and V_{loop} is the sample collection loop volume of GC (0.25 mL)

Moles of H_2/O_2 from GC volume:

$$\mathbf{n} = \frac{PV}{RT} \quad (2)$$

where, P (1 atm) is the pressure of dry gas, V is volume of products, T is room temperature (298.15 K) and R is ideal gas constant (0.082057).

Faradaic efficiency (F.E., %):

$$F.E._{H2}(\%) = \frac{2\, n_{H2} F}{Q} \times 100 \quad (3)$$

$$F.E._{O2}(\%) = \frac{4\, n_{O2} F}{Q} \times 100 \quad (4)$$

where, 2 and 4 are no. of electrons involved during HER and OER, respectively, whilst n is the respective no. of moles, F is Faraday constant (96485 C mol-1) and Q is the charge passed during electrolysis (from chronopotentiometry curve).

Product yield rate (μ mol g^{-1} h^{-1}):

$$r_{H2/O2} = \frac{n_{H2/O2}}{t \times m} \quad (5)$$

where, t is the time of electrolysis and m is the mass loading of catalyst.

Table S1. Metal contents (wt. %) of spent black mass and optimized leaching residue and leaching efficiency (%).

Samples	**wt.%**			
	Li	**Mn**	**Co**	**Ni**
Black mass	4.87	7.57	14.34	17.69
Leaching residue	0.24	10.1	25.2	63.3
Leaching efficiency (%)	96.64	26.34	1.71	1.26

Table S2. Residual metal concentrations in ethanol washed solutions after DES removal from leaching residue.

Metal Concentration (ppm)	**Leachate**	**Ethanol washed solution**		
		1st wash	**2nd wash**	**3rd wash**
Li	1397	309	134	52
Co	41	22	16	7
Ni	84	35	20	12
Mn	399	184	105	47

Table S3. Mass ratio (wt.%) of critical metals in catalysts calcined at different temperatures.

Calcination temperature (°C)	**wt.%**			
	Li	**Ni**	**Co**	**Mn**
700	0.45	36.32	24.56	4.84
800	0.43	42.17	41.72	14.63
900	0.97	42.20	33.02	8.66

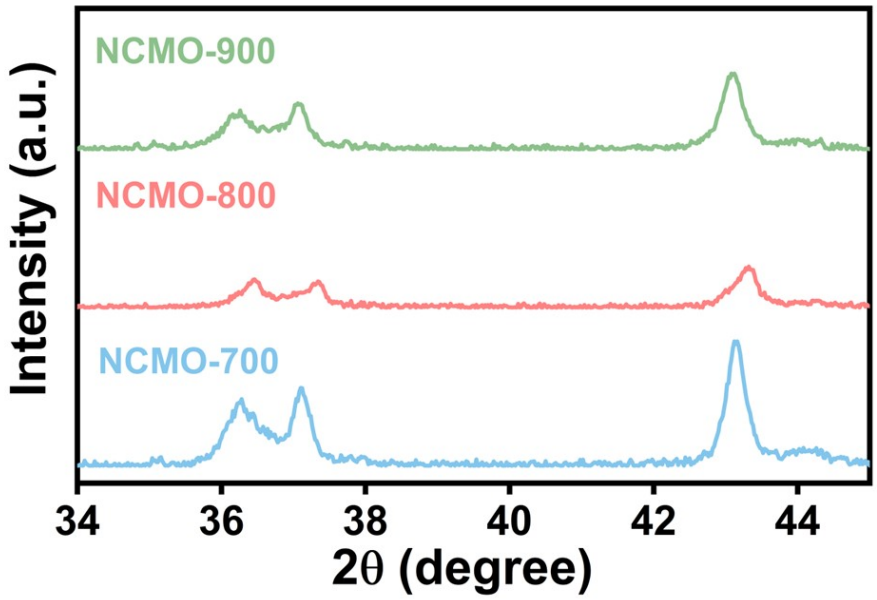

Fig. S1 X-ray diffraction patterns for NCMO-T catalysts showing peak broadening and intensity reduction with increased calcination temperature.

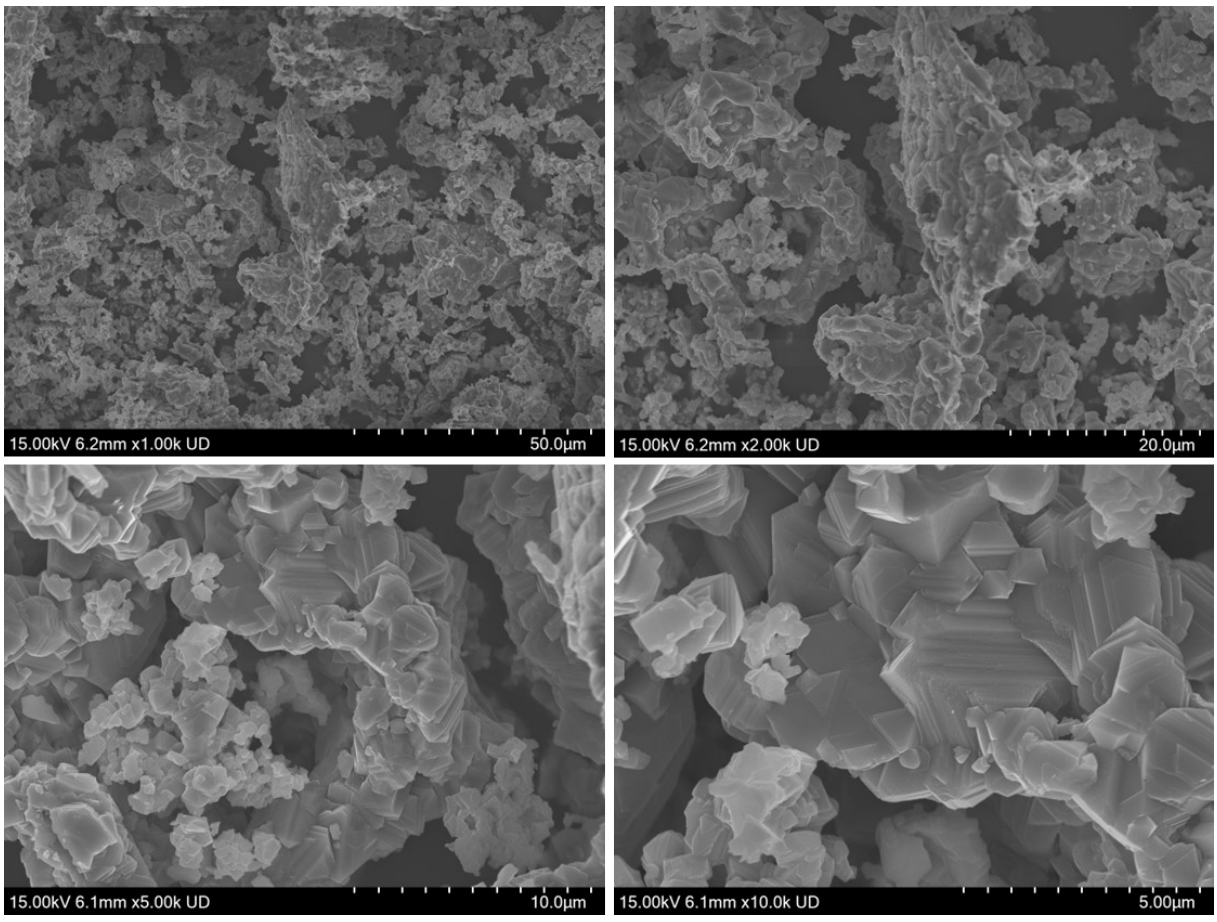

Fig. S2 FE-SEM images of the calcinated NCMO-700 catalyst at different magnifications.

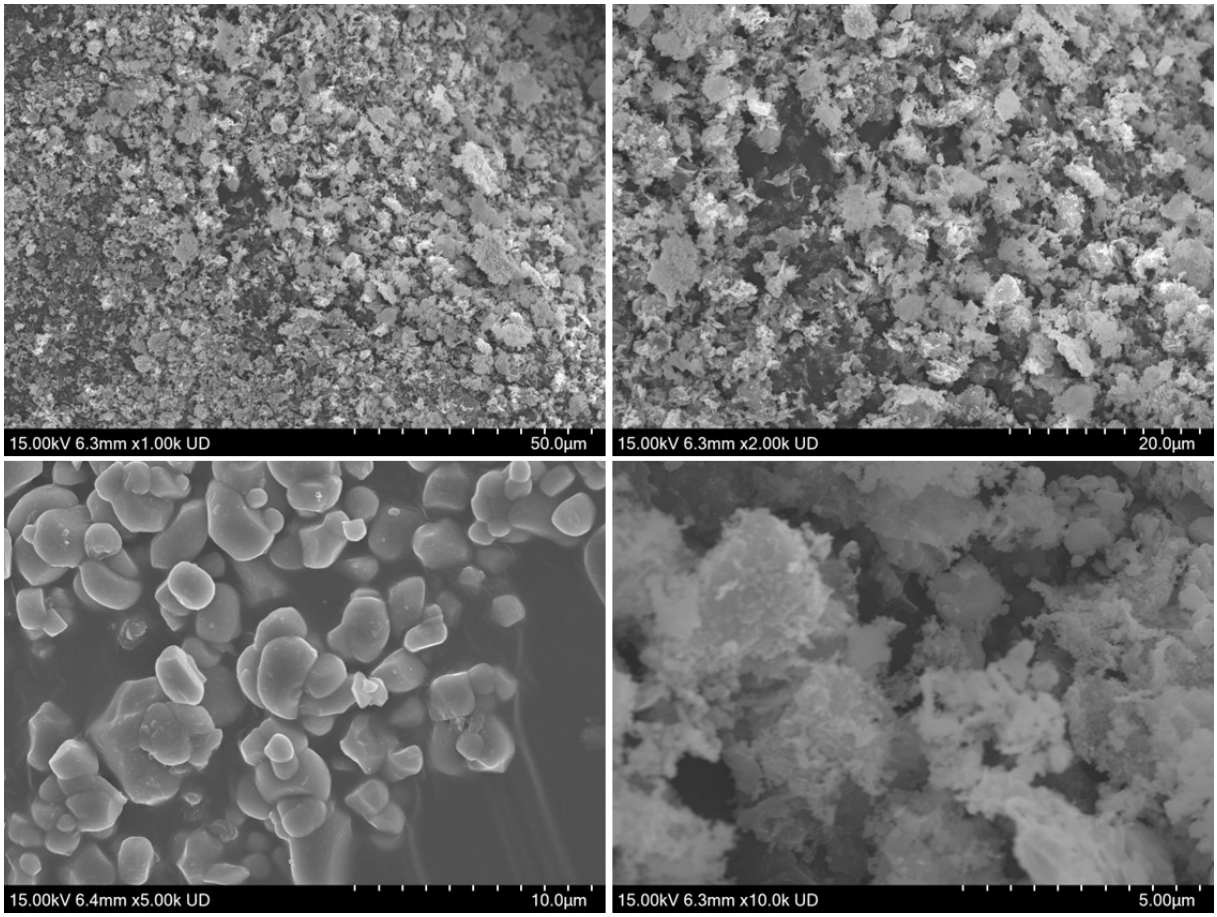

Fig. S3 FE-SEM images of the calcinated NCMO-900 catalyst at different magnifications.

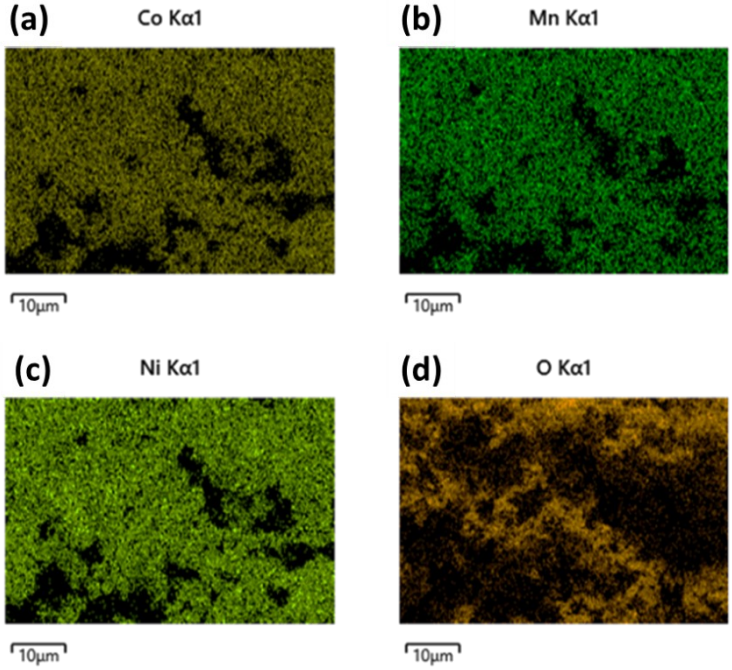

Fig. S4 Elemental mapping images of NCMO-700 catalyst showing the presence of **(a)** Co, **(b)** Mn, **(c)** Ni and **(d)** O respectively.

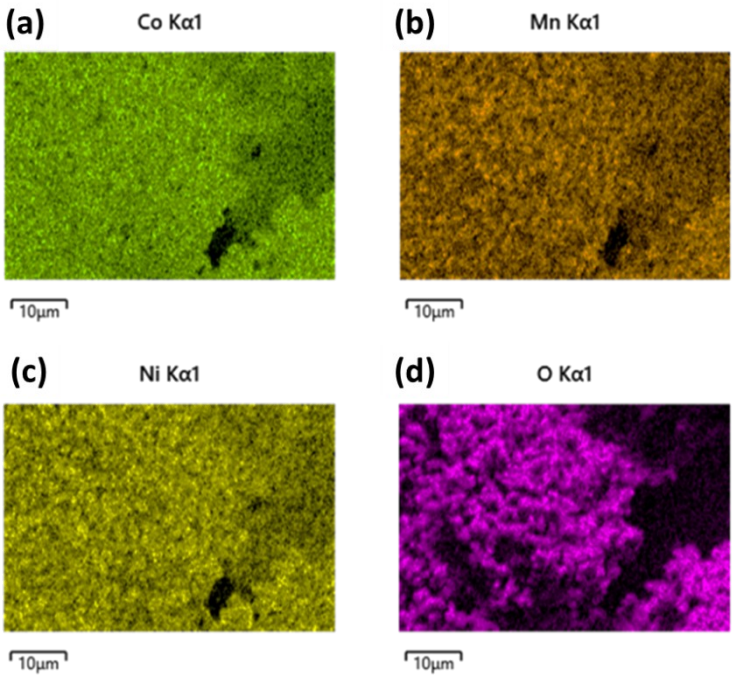

Fig. S5 Elemental mapping images of NCMO-800 catalyst showing the presence of **(a)** Co, **(b)** Mn, **(c)** Ni and **(d)** O respectively.

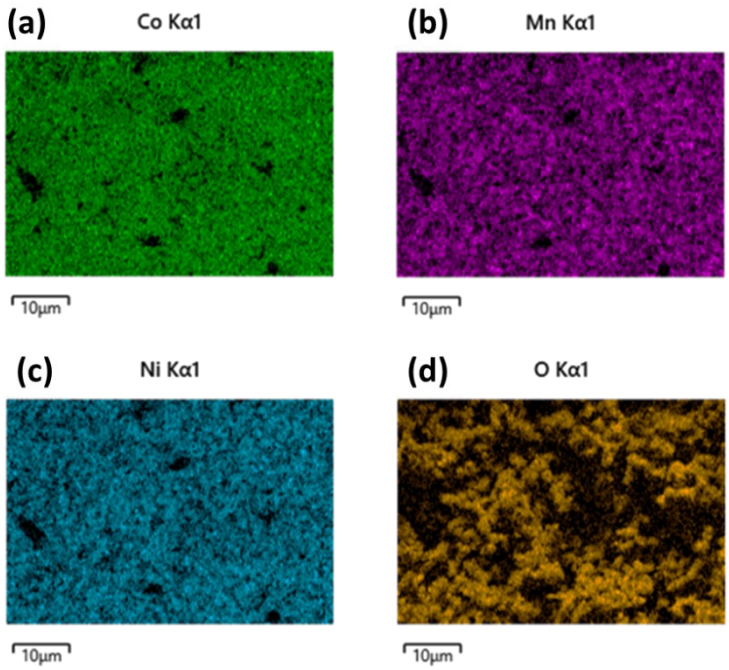

Fig. S6 Elemental mapping images of NCMO-900 catalyst showing the presence of **(a)** Co, **(b)** Mn, **(c)** Ni and **(d)** O respectively.

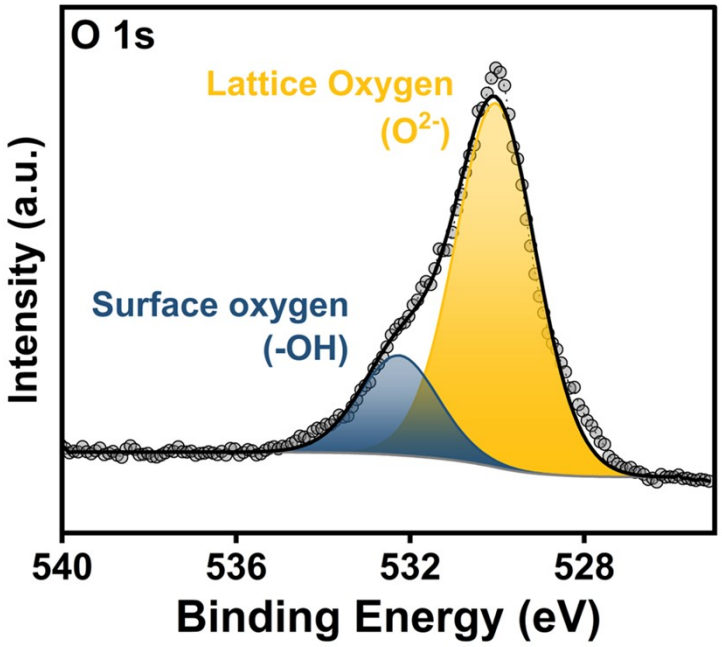

Fig. S7 Deconvoluted O 1s XPS spectrum for NCMO-800 catalyst before electrolysis.

Table S4. Comparison of current density and overpotential of NCMO-T and benchmark RuO_2 during OER in 1 M KOH.

S. No.	Catalyst	Current density at 1.9 V vs. RHE ($mA\ cm^{-2}$)	Overpotential at 10 $mA\ cm^{-2}$ (mV)
1.	NCMO-700	13.6	570
2.	NCMO-800	149.5	330
3.	NCMO-900	32.2	470
4.	RuO_2	119.6	310

Table S5. EIS calculations for NCMO-T catalysts at OER potential, extracted from Fig. 3c.

S. No.	Catalyst	*Rs* (Ω)	R_{ct} (Ω)

1.	NCMO-700	2.975	39.505
2.	NCMO-800	2.63	13.48
3.	NCMO-900	3.03	24.34

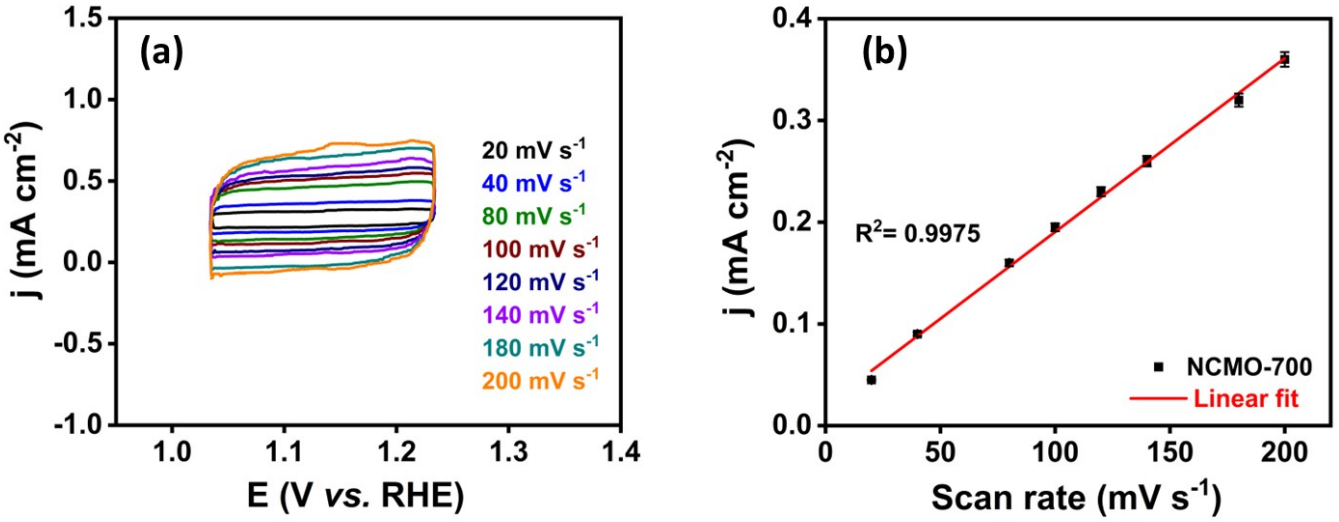

Fig. S8 (a) Cyclic voltammograms acquired under non-faradaic region at varying scan rates and **(b)** corresponding linear plot between scan rate and average current density extracted from CVs for NCMO-700 catalyst.

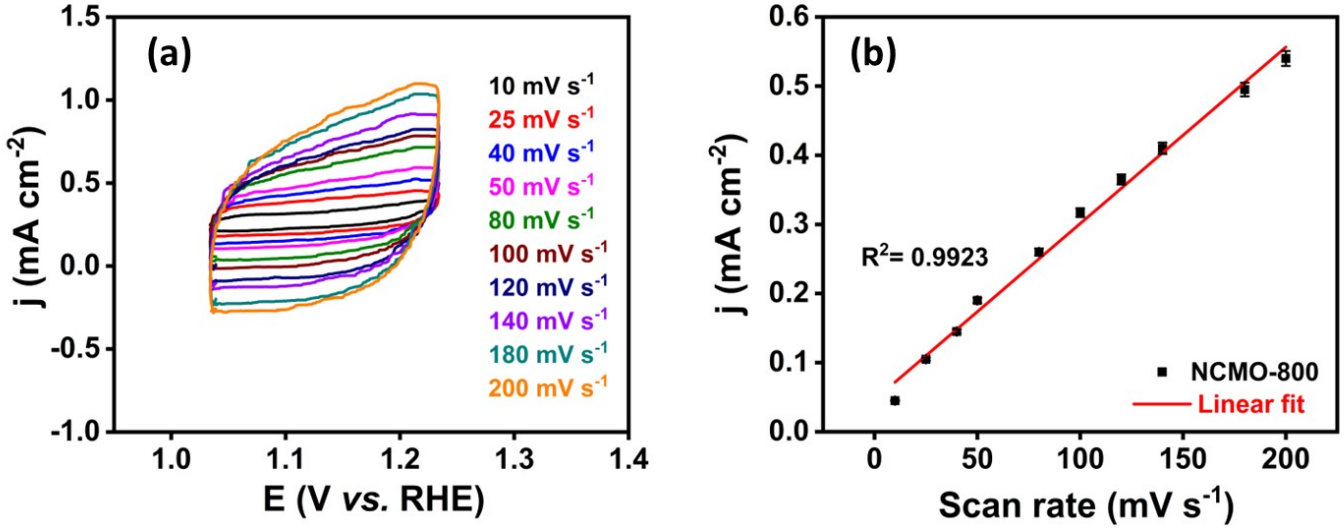

Fig. S9 (a) Cyclic voltammograms acquired under non-faradaic region at varying scan rates and **(b)** corresponding linear plot between scan rate and average current density extracted from CVs for NCMO-800 catalyst.

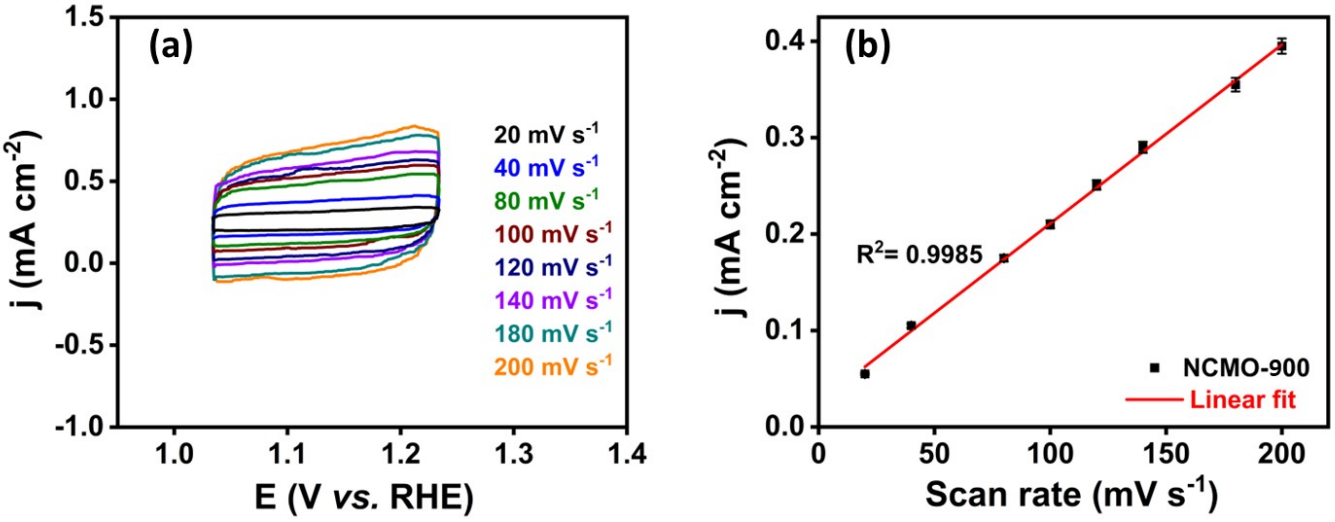

Fig. S10 (a) Cyclic voltammograms acquired under non-faradaic region at varying scan rates and **(b)** corresponding linear plot between scan rate and average current density extracted from CVs for NCMO-900 catalyst.

Table S6. ECSA calculations for NCMO-T catalysts.

S. No.	Electrocatalyst	C_{dl} (mF) at 1.1 V *vs.* RHE	ECSA (cm^2)
1.	NCMO-700	1.71	42.75
2.	NCMO-800	2.55	63.75
3.	NCMO-900	1.86	46.5

Table S7. Comparison of current density and overpotential of NCMO-T and benchmark Pt/C during HER in 1 M KOH.

S. No.	Catalyst	Current density at -0.6 V *vs.* RHE ($mA\ cm^{-2}$)	Overpotential at 10 $mA\ cm^{-2}$ (mV)
1.	NCMO-700	32.2	351
2.	NCMO-800	82.5	193
3.	NCMO-900	47.3	289

4.	Pt/C	193.4	153

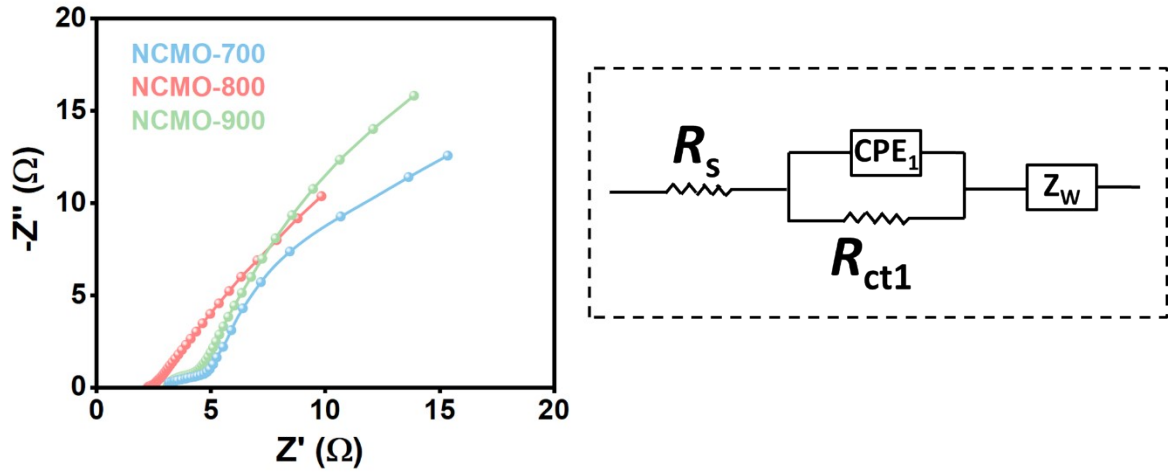

Fig. S11 Nyquist plots for NCMO-T catalysts under HER potential (-0.2 V vs. RHE) with corresponding equivalent circuit.

Table S8. EIS calculations for NCMO-T catalysts at HER potential, extracted from Fig. S8.

S. No.	**Catalyst**	***Rs* (Ω)**	**R_{ct} (Ω)**
1.	NCMO-700	3.1	1.62
2.	NCMO-800	2.18	0.34
3.	NCMO-900	3.08	0.91

Table S9. Water contact angle dataset for NCMO-700

Time [s]	CA mean [°]	Volume [Î¼l]	Baseline [mm]
0	-	-	-
0.17	15.74	0	3.54
0.5	15.01	0	3.58
0.67	14.61	0	3.6
0.83	14.11	0	3.63
1	14.99	0	3.63
1.17	14.58	0	3.64
1.33	12.71	0.08	3.62
1.5	12.67	0.03	3.7
1.67	12.32	0.13	3.72
1.83	11.88	0.33	3.79
2	11.5	0.4	3.8
2.17	11.12	0.49	3.84
2.67	6.67	0.64	3.73
9.16	4.64	0.52	3.77
9.33	4.71	0.56	3.96
9.5	4	0.57	4.08
9.66	3.99	0.41	3.92
9.83	5.2	0.07	1.99

Table S10. Water contact angle dataset for NCMO-800

Time [s]	CA mean [Â°]	Volume [Î¼l]	Baseline [mm]
0	6.78	1.33	5.14
0.17	5.72	1.46	5.23
0.33	8.62	0.74	4.66
0.5	5.1	1.11	5.24
0.67	3.89	0.82	5.02
0.83	2.84	0.75	5.34

Table S11. Water contact angle dataset for NCMO-900

Time [s]	CA mean [Â°]	Volume [Î¼l]	Baseline [mm]
0	-	-	-
0.17	15.74	0	3.54
0.5	15.01	0	3.58
0.67	14.61	0	3.6
0.83	14.11	0	3.63
1	14.99	0	3.63
1.17	14.58	0	3.64
1.33	12.71	0.08	3.62
1.5	12.67	0.03	3.7
1.67	12.32	0.13	3.72
1.83	11.88	0.33	3.79
2	11.5	0.4	3.8
2.17	11.12	0.49	3.84
2.67	6.67	0.64	3.73
9.16	4.64	0.52	3.77
9.33	4.71	0.56	3.96
9.5	4	0.57	4.08
9.66	3.99	0.41	3.92
9.83	5.2	0.07	1.99

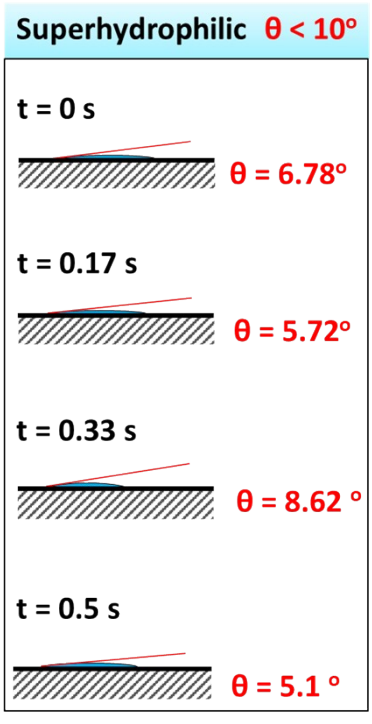

Fig. S12 Schematic representation of water contact angle and surface wettability changes over time in NCMO-800 catalyst.

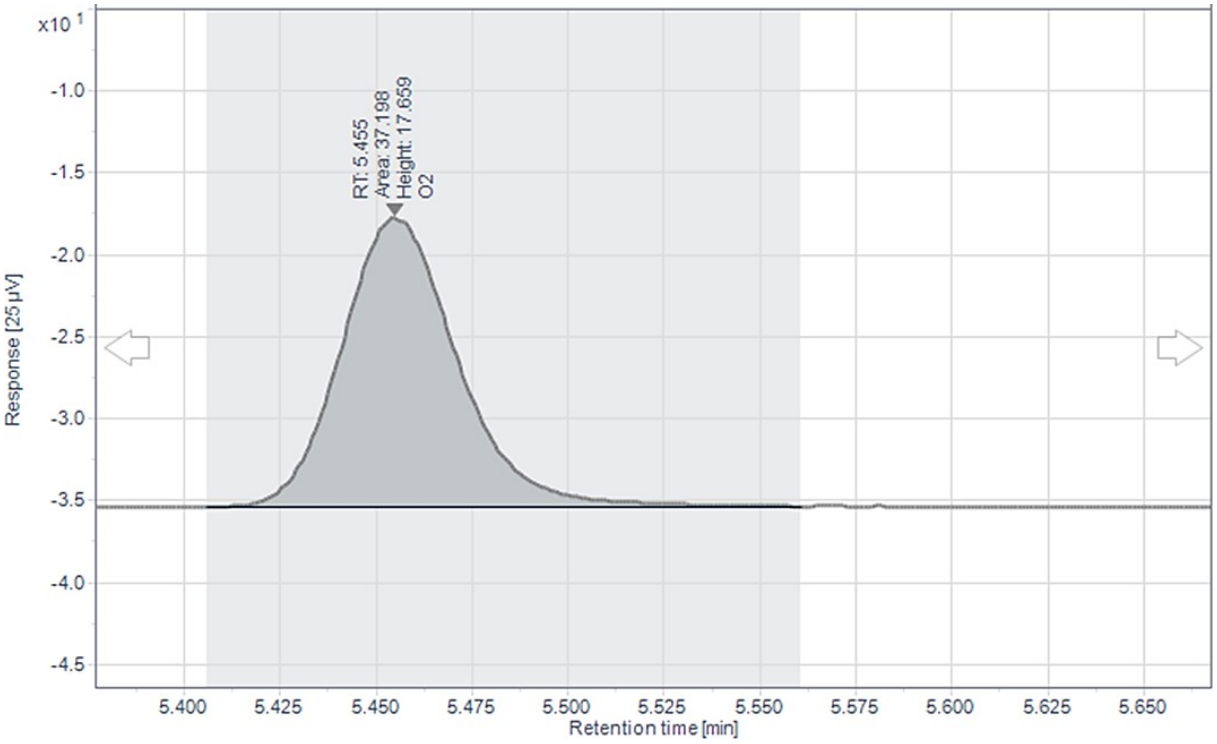

Fig. S13 Gas chromatogram obtained after OER used for O_2 quantification.

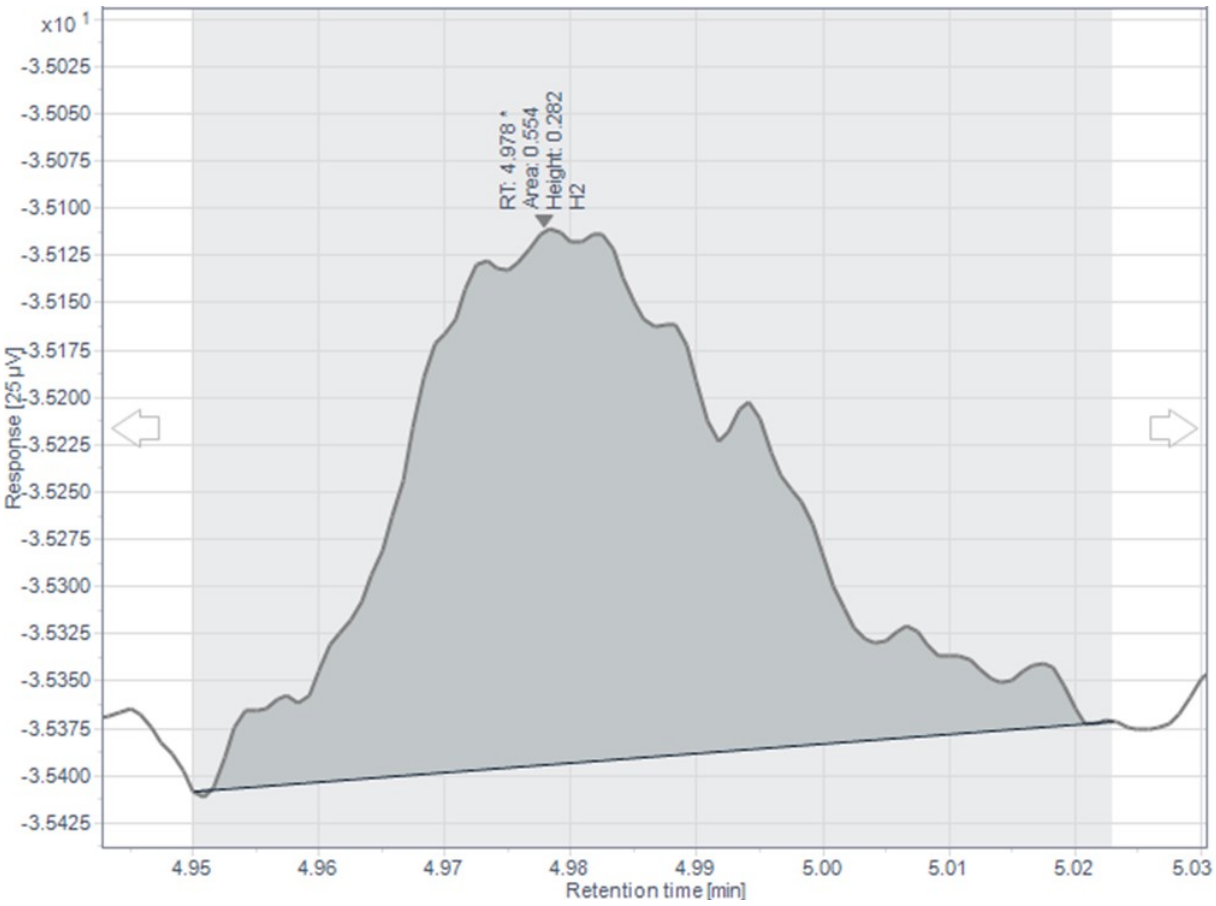

Fig. S14 Gas chromatogram obtained after HER used for H_2 quantification.

Table S12. Quantification details for O_2 signal detected during OER in GC.

Name	Signal description	RT (min)	Area	Height	Concentration
O_2	TCD1A	5.455	37.198	17.659	1.124

Table S13. Quantification details for H_2 signal detected during HER in GC.

Name	Signal description	RT (min)	Area	Height	Concentration
H_2	TCD1A	4.978	0.554	0.282	0.135

Table S14. ICP-MS analysis for metal concentration in electrolyte after 24 h stability tests.

Catalyst	**Metal concentration (ppb)**		
	Mn	**Co**	**Ni**
NCMO-800	< 0.048	<0.035	0.3033

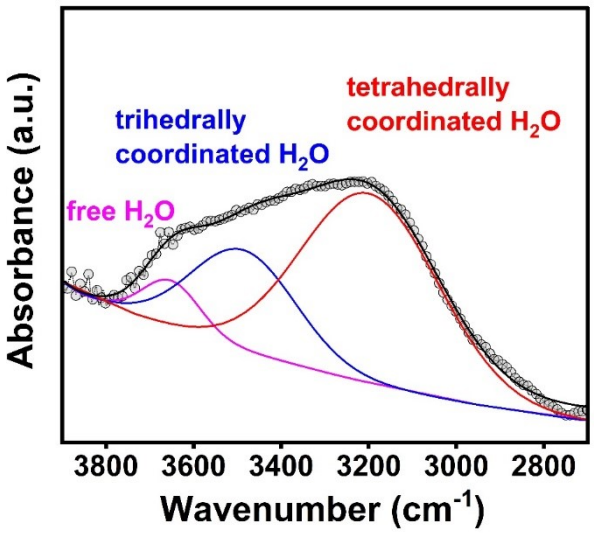

Fig. S15 Deconvoluted *in-situ* FTIR spectra for O-H band at -0.5 V, showing HER over NCMO-800 catalyst.

Table S15. Comparison of bifunctional OER-HER activity with Ni, Co and Mn-based oxides in literature.

Catalyst	Electrolyte	OER		HER	
		Current density (mA cm^{-2})	Overpotential (mV)	Current density (mA cm^{-2})	Overpotential (mV)
NCMO-800 (This work)	**1 M KOH**	**10**	**320**	**10**	**193**
CNM-811[4]	1 M NaOH	30	338	10	190
NP-$NiCo_2O_4$[5]	1 M KOH	10	410	10	370
$Co_{2.1}Mn_{0.9}O_4$[6]	1 M KOH	20	425	-	-
Co_3O_4/NF-Ar/O_2[7]	1 M KOH	20	269	10	135
Co_3O_4/CC[8]	0.1 M KOH/0.1 M H2SO4	10	357	10	291
Co_3O_4 NCs@NSs[9]	0.1 M KOH	10	460	10	363
NIM-175[10]	1 M KOH	10	250	10	248
$NiCo_2O_4$[11]	1 M KOH	10	310	10	106
$NiCo_2O_4$-Chitosan[12]	1 M NaOH	10	310	10	240
NFCO-Na[13]	1 M KOH	10	248	10	153
NCO-NSs[14]	1 M KOH	10	230	10	170
$Ni_{0.8}Mn_{0.2}Co_2O_4$[15]	1 M KOH	10	123	10	150
Mn doped Co_3O_4[16]	1 M KOH	10	265	10	157
NCO/CO-500[17]	1 M KOH	10	274	10	163

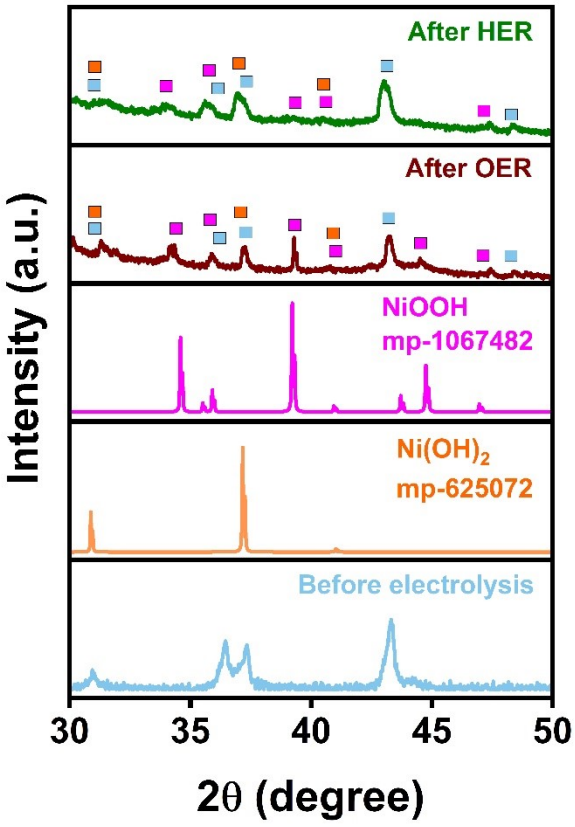

Fig. S16 X-ray diffraction patterns acquired for NCMO-800 catalyst after OER and HER, compared with XRD of NCMO-800 before electrolysis and reference nickel hydroxide (*Data retrieved from the Materials Project for $Ni(HO)_2$ (mp-625072) from database version v2025.09.25*) and oxyhydroxide (*Data retrieved from the Materials Project for $NiHO_2$ (mp-1067482) from database version v2025.09.25*) diffraction patterns.

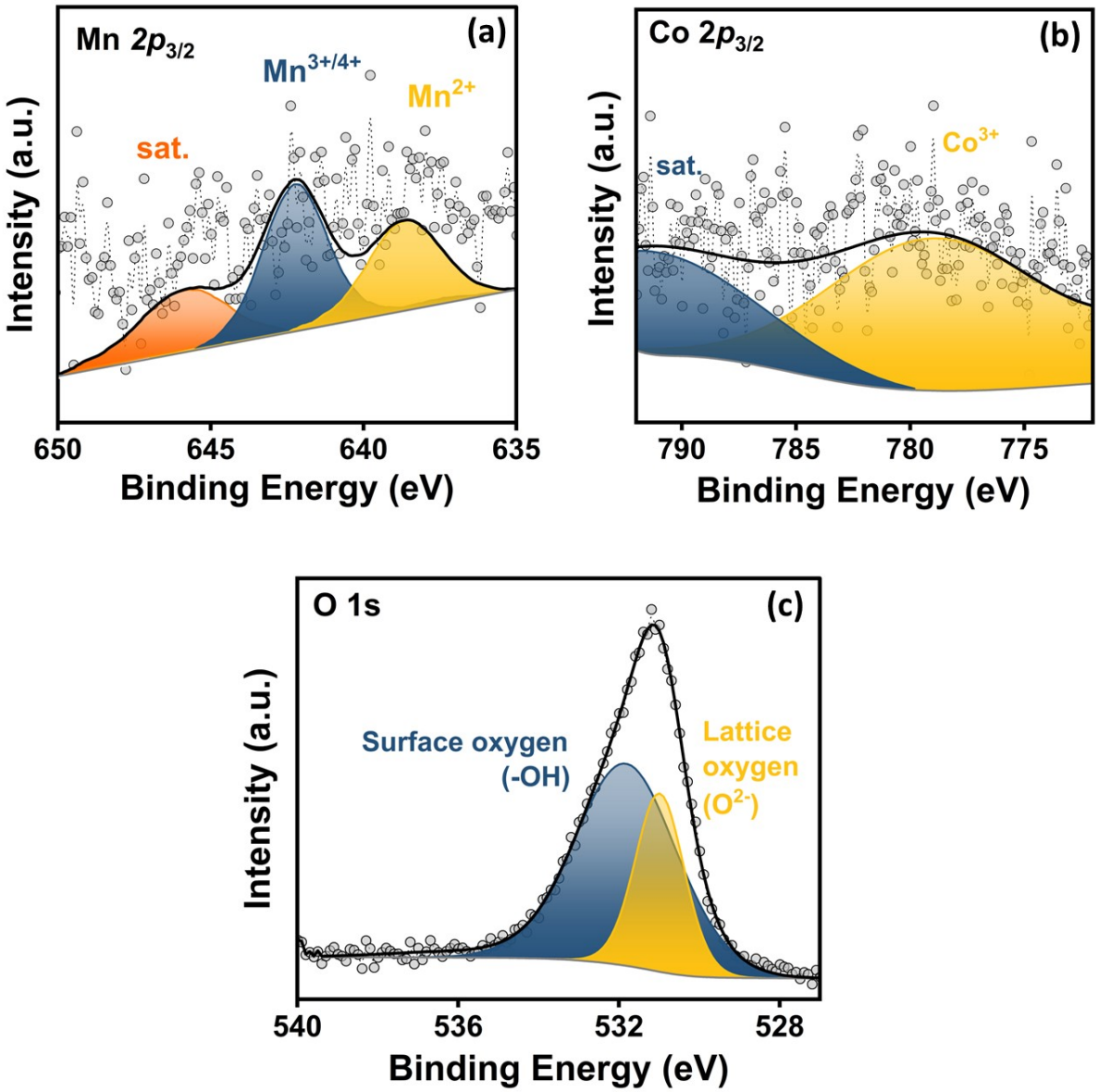

Fig. S17 Deconvoluted **(a)** Mn 2p, **(b)** Co 2p and **(c)** O 1s XPS spectrum for NCMO-800 after OER.

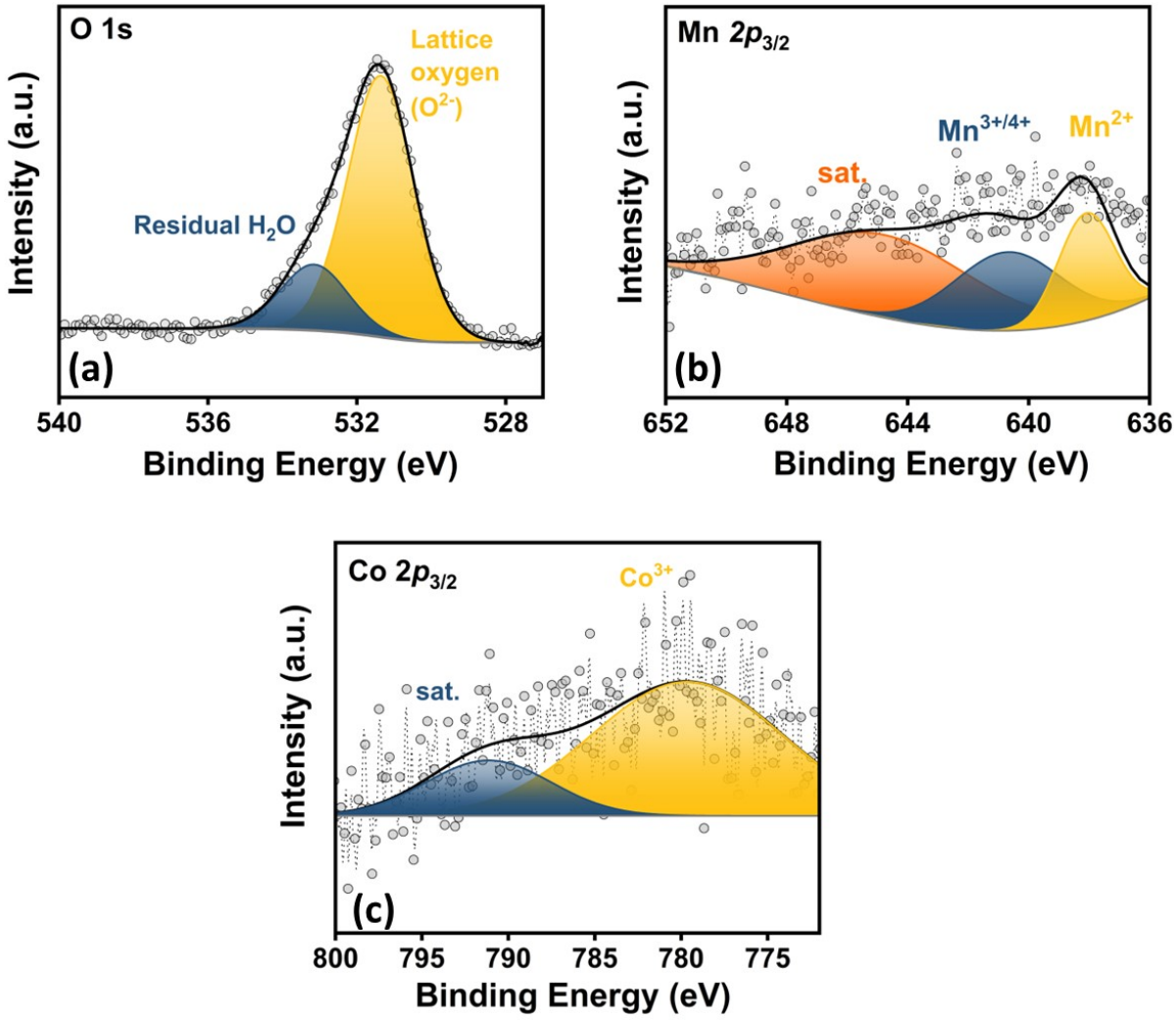

Fig. S18 Deconvoluted **(a)** O 1s, **(b)** Mn 2p and **(c)** Co 2p XPS spectrum for NCMO-800 after HER.

References

1. J. Wang, J. Yuwono, Y. Wang, Y. Lyu, S. Liu, T. Hall, R. Zeng, J. Mao and Z. Guo, *Advanced Science*, 2025, e14509.
2. Z. Zhang, T. Trần-Phú, J. Yuwono, Z. Ma, Y. Yang, J. Leverett, R. K. Hocking, B. Johannessen, P. Kumar and R. Amal, *Applied Catalysis B: Environment and Energy*, 2025, **371**, 125203.
3. G. Zhang, P. Ranjith, Z. Li, J. Vongsvivut and M. Gao, *Fuel*, 2021, **296**, 120639.
4. J. Lin, Y. Ding, H. Jin and T. Zeng, *Ionics*, 2024, **30**, 2287-2298.
5. R. Elakkiya, R. Ramkumar and G. Maduraiveeran, *Materials Research Bulletin*, 2019, **116**, 98-105.
6. J. Lin, Y. Ding, H. Jin and T. Zeng, *Catalysts*, 2023, **13**, 1031.
7. F. Chen, R. Zhang, Y. Zhang, X. Hao, Y. Liu, M. Xu, C. Sun, Y. Song, G. Gao and H. Dong, *Applied Surface Science*, 2024, **657**, 159839.
8. H. P. P. La, K. T. T. Tran, L. B. H. Nguyen, M. Van Tran and V. Van Pham, *International Journal of Hydrogen Energy*, 2024, **52**, 482-493.
9. N. Bhuvanendran, M. G. Choi, D. Kim and S. Y. Lee, *Journal of Alloys and Compounds*, 2023, **935**, 168079.
10. P. Nagajyothi, K. Pavani, R. Ramaraghavulu and J. Shim, *International Journal of Hydrogen Energy*, 2024, **54**, 691-699.
11. T. Kavinkumar, T. Naveenkumar and A. Thirumurugan, *Inorganic Chemistry Communications*, 2024, **165**, 112582.
12. S. S. Medany, A. Nafady, R. A. Soomro and M. A. Hefnawy, *Scientific Reports*, 2024, **14**, 2453.
13. S. C. Jesudass, S. Surendran, D. J. Moon, S. Shanmugapriya, J. Y. Kim, G. Janani, K. Veeramani, S. Mahadik, I. G. Kim and P. Jung, *Journal of Colloid and Interface Science*, 2024, **663**, 566-576.
14. L. Tao, Y. Li, M. Li, G. Gao, X. Xiao, M. Wang, X. Jiang, X. Lv, Q. Li and S. Zhang, *The Journal of Physical Chemistry C*, 2017, **121**, 25888-25897.
15. S. K. Shinde, S. S. Karade, N. C. Maile, H. M. Yadav, A. D. Jagadale, M. B. Jalak and D. Y. Kim, *International Journal of Energy Research*, 2022, **46**, 16693-16715.
16. L. Zhang, F. Wei and H. Liang, *Materials Today Communications*, 2024, **40**, 109887.
17. R. R. Ayyaluri, O. R. Ankinapalli and J. S. Yu, *International Journal of Hydrogen Energy*, 2025, **148**, 150048.